Bubble size distribution and stability of CO_2 microbubbles for enhanced oil recovery: effect of polymer, surfactant and salt concentrations

Nam Nguyen Hai Le
Department of Earth Resources Engineering, Kyushu University

Sugai, Yuichi
Department of Earth Resources Engineering, Faculty of Engineering, Kyushu University

Nguele, Ronald
Department of Earth Resources Engineering, Kyushu University

Sreu, Tola
Department of Earth Resources Engineering, Kyushu University

出版情報：Journal of Dispersion Science and Technology, 2021-09-10. Taylor and Francis
バージョン：
権利関係：

Bubble size distribution and stability of CO_2 microbubbles for enhanced oil recovery: Effect of polymer, surfactant and salt concentrations

Nam Nguyen Hai Le[a,b,c]*, Yuichi Sugai[a], Ronald Nguele[a], and Tola Sreu[a]

[a]*Department of Earth Resources Engineering, Kyushu University, Fukuoka, Japan*
[b]*Faculty of Geology and Petroleum Engineering, Ho Chi Minh City University of Technology (HCMUT), 268 Ly Thuong Kiet Street, District 10, Ho Chi Minh City, Vietnam*

[c]*Vietnam National University Ho Chi Minh City, Linh Trung Ward, Thu Duc District, Ho Chi Minh City, Vietnam*

*corresponding author: Nam Nguyen Hai Le, email: inhnam@mine.kyushu-u.ac.jp

Abstract

Fluids incorporating carbon dioxide (CO_2) microbubbles have been utilized to promote enhanced oil recovery from hydrocarbon reservoirs. The performance of such fluids in porous media is greatly affected by both the bubble size and stability. On this basis, the present study evaluated the effects of varying the concentrations of a xanthan gum (XG) polymer, a surfactant (sodium dodecyl sulfate: SDS) and sodium chloride (NaCl) on both the stability and bubble size distribution (BSD) of CO_2 microbubbles. CO_2 microbubble dispersions were prepared using a high-speed homogenizer in conjunction with the diffusion of gaseous CO_2 through aqueous solutions. The stability of each dispersion was ascertained using a drainage test, while the BSD was determined by optical microscopy and fitted to either normal, log-normal or Weibull functions. The results showed that a Weibull distribution gave the most accurate fit for all experimental data. Increases in either the SDS or XG polymer concentration were found to decrease the microbubble size. However, these same changes increased the microbubble stability as a consequence of structural enhancement. The addition of NaCl up to a concentration of 10 g/L (10g/1000g) decreased the average bubble size by approximately 2.7%. Stability was also reduced as the NaCl concentration was increased because of the gravitational effect and coalescence.

Graphical Abstract

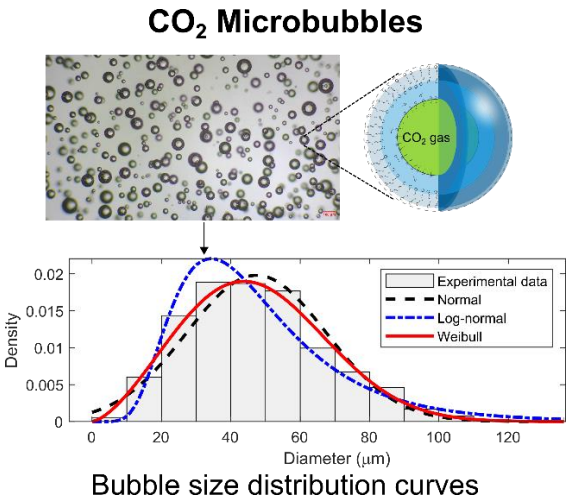

KEYWORDS: CO_2 microbubbles, colloidal gas aphrons, bubble size distribution, stability, enhanced oil recovery

1 INTRODUCTION

The advantages of employing carbon dioxide (CO_2) as a displacement agent during enhanced oil recovery (EOR) have received significant attention in the petroleum industry. An additional benefit is that this method would provide an economical approach to the geological storage of CO_2 to reduce atmospheric CO_2 concentrations [1–5]. However, CO_2 flooding can result in low recovery efficiencies because of the high mobility of CO_2 in flooding areas. Specifically, the injected CO_2 tends to flow through highly permeable layers or fractures, which leads to poor sweeping efficiency in the low permeability zones [6]. The use of CO_2 foams has been shown to provide suitable mobility control and to improve the sweeping efficiency during CO_2-based EOR, by increasing the gas viscosity and diverting fluid to low permeability layers. Unfortunately, these foams tend to become unstable in high-temperature, high-pressure environments, and this lack of stability is a challenge with regard to EOR applications [7]. Recently, microbubbles (defined as having sizes of 10 to 100 μm) have become of interest as a means of removing contaminants from aqueous solutions [8, 9], as components of oil well-drilling fluids [10–14] and also with regard to EOR [15–17]. The use of microbubble-based fluids is growing rapidly in the oil and gas industry. One advantage of microbubbles is that they have a unique structure differing from that of conventional foams that maintains their stability for longer time periods under severe conditions. The first report of microbubbles in colloidal gas aphrons (CGAs) was by Sebba [18]. CO_2 microbubbles comprise a spherical core made of gaseous CO_2 with a multilayer covering comprising surfactant molecules and a viscous liquid. This multilayer structure, made of an inner layer (between the gaseous core and the liquid layer) and an outer double layer of surfactant, acts as a barrier against the bulk liquid. The microbubble shell reduces the migration of gas from the core to the bulk phase. As

a result, gas diffusivity is lowered and these foams are more stable than conventional foams, in which the bubbles comprise a spherical gas core with a surfactant layer [19]. To date, several studies have demonstrated the remarkable stability of microbubble-based foams compared with conventional foams. Ivan et al. [20] examined the effect of elevated pressure on CGAs and found that these foams remained stable up to a pressure of 10.3 MPa, while Growork [21] demonstrated that CGAs could survive for a significant time span under pressurization as high as 27.6 MPa. Bjorndalen [22] visually assessed the stability of CGAs and the corresponding bubble sizes at high pressures and found that the foams were stable but that the microbubble size decreased with increasing pressure up to 3.4 MPa. Pasdar et al. [23] investigated CGAs during compression and decompression and reported that these materials were stable up to 13.7 MPa, while Bjorndalen [22] showed that CGAs became unstable at temperatures ranging from 50 to 75 °C.

Several studies have indicated that microbubbles can seal highly permeable layers in heterogeneous porous media during the EOR process, and so improve sweeping efficiency and oil recovery. Yang et al. applied a microbubble foam to shallow reservoirs and concluded that these microbubbles blocked porous media via the Jamin effect [24]. As a microbubble flows through a pore, it will experience a capillary force if its diameter is larger than the pore throat [25]. Shi et al. [16] conducted double sandpack experiments and determined that microbubbles blocked the high permeability sandpack while increasing the swept volume in the sandpack with lower permeability. Shi et al. [26] attempted a micromodel test of plugging performance and showed that microbubbles were capable of temporarily plugging the highly permeable regions such that subsequent flow was forced into the low permeability areas.

Telmadarreie et al. [19] focused on the effectiveness of employing CO_2 microbubbles as

an injection agent to improve heavy oil recovery based on flooding tests in heterogeneous porous media. The results showed that injecting CO_2 microbubbles significantly increased the sweeping efficiency relative to the performance of the base fluid. Andi et al. [15] performed EOR flooding tests in parallel sandpacks using CO_2 microbubbles. They observed that these microbubbles blocked pores in the high permeability sandpack, therefore improving the displacement efficiency in the low permeability sandpack and increasing the cumulative oil production.

The blocking performance of microbubbles is greatly affected by their stability and size distribution. Longe [27] and Jauregi et al. [28] evaluated the effects of the amount of surfactant on the stability of CGAs, and both concluded that increasing the surfactant concentration improved the CGA stability. Pasdar et al. [29] showed that increased viscosity also enhanced the stability of CGAs. Arabloo et al. [30] performed static drainage tests and observed that the amount of a xanthan gum (XG) polymer in the CGA dispersion played an essential role in conferring stability. Overall, the stability of microbubbles appears to be greatly affected by the concentrations of both polymers and surfactants in the foam.

Both static liquid drainage [31, 32] and bubble size distribution [33] can be used to assess the stability of microbubbles. The static liquid drainage methods measure the liquid phase volume drained from the microbubble system as a function of time, and several researchers have used this technique to study the stability of CGAs. Yan et al. [31] proposed an empirical model to characterize the liquid drainage from CGA dispersions, while Sadeghialiabadi and Amiri [34] investigated the effects of geometric and operating variables on CGA stability using the drainage curve method. Amir et al. [35] also studied the stability of nano-enhanced CGAs by monitoring drainage rates. In contrast, the bubble size distribution technique evaluates increases in bubble size over

time as a measure of stability. Several methods have been developed to ascertain bubble size distribution, including visual, electro-resistivity and acoustic techniques [36].

Visual methods (including microscopy, photography and video microscopy) are most frequently used to measure particle and bubble size distributions [37, 38]. Optical microscopy in particular has been widely employed to ascertain the size and stability of CGAs. As an example, Zhu et al. [10] determined the bubble size distribution and examined the effect of attapulgite on CGA drilling fluid stability using optical microscopy in conjunction with a Gaussian statistical distribution. Parmar et al. [39] generated a microbubble suspension by transferring a mixture of gas and liquid to a pressure chamber and found a Weibull distribution of bubble sizes based on image analysis. It should be noted that neither of the above two studies employed a goodness of fit test to determine which mathematical distribution function best represented the experimental data. Raquibul [40] proposed that the bubbles produced in a laboratory-scale electroflotation cell had a log-normal diameter distribution based on a high goodness of fit. Nevertheless, few reports to date have examined the size distributions of CO_2 microbubbles intended for EOR.

In addition, there is still disagreement concerning the effects of the surfactant on the microbubble diameter distribution. Xu et al. [41] reported that increases in the surfactant concentration decreased the bubble diameter, in contrast to the statement that the size of CGA microbubbles increased with increasing surfactant concentrations [33, 42]. Bjorndalen also showed that, at surfactant concentrations lower than the critical micelle concentration (CMC), increments in the amount of surfactant decreased the CGA bubble size [22]. The contradiction in these results shows the necessity of performing additional work to study the effects of surfactant concentration on microbubble size. There is also a need for an efficient means of reducing experimental

uncertainty when investigating the size distributions of CO_2 microbubbles.

The present research examined the effects of the polymer, surfactant and salt concentrations on the stability of CO_2 microbubbles using drainage tests. This work also employed microscopic imaging together with statistical interpretation to determine the effects of the above parameters on the microbubble size distribution. A further objective of this study was to obtain a better understanding of the variations in CO_2 microbubble diameter distributions.

2 EXPERIMENTAL

2.1 Materials

In this study, the anionic surfactant sodium dodecyl sulfate (SDS, purity> 99.8%) was used for the generation of microbubbles. This surfactant was selected based on literature reports that it allows the successful generation of CGAs [10, 15, 42]. A xanthan gum (XG) biopolymer was also employed as a microbubble stabilizer and sodium chloride (NaCl) was added to examine the effect of salinity on the CGAs. All chemicals were supplied by Junsei Chemical (Japan) and deionized (DI) water was used to prepare all aqueous solutions.

2.2 Methods

2.2.1 Preparation of base solutions

A series of saline solutions was prepared by dissolving specific amounts of NaCl in 300 mL DI water. The base solutions were then obtained by adding varying amounts of the SDS and XG polymer to these saline solutions, followed by stirring for 2 h using a magnetic stirrer at 1000 rpm to achieve complete dissolution.

2.2.2 Preparation of CO_2 microbubble dispersions

Figure 1 presents a diagram showing the apparatus used to generate CO_2 microbubbles. In this process, 200 mL of a base solution was transferred into a 300 mL container, after which CO_2 gas (99.9% pure) was injected from the bottom of the container through a diffuser at a flow rate of 15 mL/min using a flow controller. The dispersion was subsequently homogenized by stirring at a rate of 8000 rpm for 4 min using an overhead mixer. The gaseous CO_2 diffused into the base solution eventually broke down into microbubbles with micron-scale diameters. All experiments were performed at ambient temperature and pressure.

2.2.3 CO_2 microbubble stability assessments

In preparation for stability tests, a quantity of each CO_2 microbubble dispersion was transferred into a 300-mL graduated cylinder and allowed to stand. As time passed, the aqueous solution drained from the microbubbles and the volume of this solution was recorded over time. The maximum volume of drained liquid (200 mL) was obtained at the point at which the CO_2 microbubbles had entirely collapsed. A kinetic model was used to quantify the base solution drainage from each CO_2 microbubble dispersion over time. This model was previously proposed by Yan et al. [31] and is based on the equation:

$$V_t = V_F \frac{t^n}{t^n + T_{1/2}^n}, \quad (1)$$

where V_t (mL) and V_F (mL) are the volume of drained solution at time t (min) and the final volume of drained solution, respectively, $T_{1/2}$ (min) is the half-life (the time required for the drained liquid to equal 50% of V_F), and n is an exponent that defines the sigmoid character of the model curve. When assessing the stability of CO_2

microbubbles, a specific drainage rate constant (*K*) can be obtained by differentiating **Equation 1** as [31]:

$$K = \frac{n}{V_F T_{1/2}}. \quad (2)$$

2.2.4 Determination of CO_2 microbubble size

The CO_2 microbubbles were visualized and the bubble size distributions were evaluated by taking small aliquots of each dispersion from the test containers immediately after preparation of the dispersion and 60 min after preparation. Each sample was transferred to a glass microscope slide. A transmitted-light microscope with a charge-couple device camera connecting to a desktop computer was used to capture digital images of the CO_2 microbubbles.

Table S1 presents the compositions of the base solutions used in determining bubble size distributions. Several images were acquired from each specimen for statistical analysis and the average diameters of the CO_2 microbubbles in these images as well as the D_{10}, D_{50} and D_{90} values were determined. Here, D_{10}, D_{50} and D_{90} represent the diameters for which 10%, 50% and 90%, respectively, of the microbubbles were smaller in size. **Figure S1** presents a diagram of the microscopy imaging system used to evaluate the CO_2 microbubbles.

The captured images were processed using the ImageJ software package after being converted to 8-bit data. During processing, a threshold was applied to distinguish the edges of the microbubbles from the background and from other microbubbles. The CO_2 microbubble sizes were then estimated using the software, examining a minimum of 1000 bubbles from each sample to ensure a representative size distribution. **Figure S2** summarizes the enhancement procedure for a typical image.

2.3 Bubble size distribution

The output data from the ImageJ software were analyzed in the MATLAB program to obtain each bubble size distribution (BSD) and were also subjected to additional statistical analysis. It was essential to determine the exact distributions and so the optimal probability distribution function (PDF) was applied to the experimentally measured size data.

Three pdfs were applied to the distributions: normal, log-normal and Weibull. A normal PDF is one that conforms to the equation [43]**:**

$$f(x) = \frac{e^{\frac{-(x-\mu)^2}{2\sigma^2}}}{\sigma\sqrt{2\pi}}, \quad (3)$$

where μ is the mean, σ is the standard deviation, and x represents the diameter of a bubble. The log-normal PDF is given by [37]:

$$f(x) = \frac{1}{x\sigma\sqrt{2\pi}} e^{\frac{-(\ln(x)-\mu)^2}{2\sigma^2}}, \quad (4)$$

where σ is the theoretical standard deviation, μ is the theoretical mean of ln(x), and x is the diameter of a bubble. The Weibull PDF can be written as [37]:

$$f(x) = ba^{-b}x^{b-1}e^{\frac{-xb}{a}}, \quad (5)$$

where x is the diameter of a bubble and a and b are shape and scale parameters, respectively.

The Anderson–Darling (AD) test can be used to evaluate the reliability of a fitting and so to identify the most suitable theoretical model for a bubble size distribution [44]. Using this technique, the lowest AD value suggests the best fit for a given dataset. Higher P-values also indicate better agreement between the data and the theoretical distribution, while a P-value less than a significance level of 5% demonstrates that the

experimental data do not conform to a particular theoretical distribution [40].

3 RESULTS AND DISCUSSION

3.1 Visualization of CO_2 microbubbles

Figure 2 presents a diagram of an aphron microbubble based on the structure proposed by Sebba along with an optical microscopy image of the present CO_2 microbubbles. As noted, CO_2 microbubbles can provide a CGA in which the microbubbles have a gaseous CO_2 core surrounding by a thin aqueous film. This thin film is made of surfactant molecules and has three layers [18]. The addition of XG polymer increases the viscosity of the outer film and so strengthens the aphron structure such that the foam can endure harsh conditions such as high pressure and temperature [45].

3.1.1 Stability trials

Figure S3 shows the experimental CO_2 microbubble drainage process and demonstrates that the dispersion separated into two phases over time. **Figure 3** plots the drainage data for solutions having varying SDS concentrations without the XG polymer as functions of time. It can be seen that all the microbubbles collapsed entirely within approximately 20 min in each case. Each plot is quite similar, which confirms that (in the absence of the XG polymer) the SDS concentration had only a minimal effect on the stability of the CO_2 microbubbles. **Figure 3** also plots K as a function of the SDS concentration and demonstrates that this parameter first decreased rapidly and then was reduced more gradually as the SDS level was increased. Specifically, increasing the SDS concentration from 1 to 3 g/L decreased K by 19.37%. A low K value is associated with more stable dispersions, and the enhanced stability observed at higher SDS concentrations can be attributed to the presence of a greater number of surfactant molecules at the bubble surfaces, which in turn strengthened the microbubble shells and provided good surface elasticity [31]. These effects delay the liquid drainage and

reduced bubble coalescence as a result of greater electrostatic repulsion between the microbubbles [28].

Figure 4 plots the drainage data over time for dispersions prepared using various XG polymer concentrations with an SDS concentration of 3 g/L. It is evident from these plots that the XG polymer concentration had a significant effect and that higher XG polymer concentrations improved stability, which means that the drainage rate constant was inversely proportional to the XG polymer concentration. Specifically, the K value decreased rapidly from 5.7×10^{-3} to 7.2×10^{-5} $mL^{-1}min^{-1}$ (a decrease by a factor of 78) as the XG polymer concentration was increased from 0 to 5 g/L. These data indicate that the XG polymer greatly reduced the rate of liquid drainage in the CO_2 microbubble dispersions. The polymer would be expected to raise the viscosity of the base solution while inhibiting gas diffusion from the core to the bulk liquid, which would consequently stabilize the microbubbles [46]. These results are consistent with earlier studies [33, 35] examining the effects of polymers on CGA stability, which demonstrated improvements in stability at higher polymer concentrations.

Figure 5 plots the drainage data as functions of time for different NaCl concentrations with SDS and XG polymer levels of 3 and 5 g/L, respectively. These results confirm that the microbubble stability was slightly increased by increasing the NaCl concentration up to 10 g/L. The addition of NaCl likely formed a condensed layer around the bubbles by reducing the electrostatic repulsion between adjacent sulfate ions, which results in more stable bubbles [41]. However, a higher concentration of NaCl in the base solution of 20 g/L reduced the stability significantly. It is also apparent that K was gradually reduced and then increased more than twofold while increasing the salinity. The high drainage rate associated with reduced stability at greater NaCl concentrations can be ascribed to an increased gravitational effect [35].

3.2 CO_2 microbubble size distribution

Figure S4 shows seven optical microscopy images of CO_2 microbubble dispersions. **Figure S5** shows the fitting results obtained using the MATLAB package when applying the normal, log-normal and Weibull distribution functions to the experimental data obtained from the CO_2 microbubble dispersions at t = 0 min. It is clear from these data that the normal and Weibull density functions provided good fits to the experimental distributions. Quantile-quantile (Q-Q) plots are also presented to demonstrate the fitting of the theoretical functions to the experimental data. A Q-Q plot is a scatter diagram produced by plotting the experimental data against expected values obtained from the fitting to the distribution. Each Q-Q plot includes a straight line at 45°. If the distribution function is identical to the experimental data, then the plot should roughly agree with this reference line. **Figure S6** provides such plots for the three theoretical distributions as applied to the seven datasets. These Q-Q plots indicate a greater departure from the reference line for all the datasets when using the normal and log-normal functions. In contrast, the Weibull distribution approximates the reference line. **Table S2** presents the AD values for the three mathematical distributions as applied to the seven CO_2 microbubble samples in this study.

For each individual dataset in **Table S2**, a Weibull distribution provided a statistically significant fitting and gave the lowest AD value. In addition, the P-values obtained from the AD calculations were consistently higher than 0.05 with Weibull distributions for all seven data sets. It can therefore be concluded that Weibull distributions best described the BSDs. In contrast, the AD values corresponding to the normal and log-normal distributions were high with very low P-values. Therefore, the BSDs of CO_2 microbubbles were not well predicted by either type of distribution.

3.3 Factors affecting the BSD of CO_2 microbubbles

3.3.1 Effect of SDS surfactant concentration

Experiments were conducted with samples having SDS concentrations of 1, 2 or 3 g/L along with a constant XG polymer concentration of 5 g/L. The images in **Figure 6** demonstrate that the bubble sizes in sample S1 were significantly larger than those in samples S2 and S3. Increasing the SDS concentration was also found to reduce the D_{50} and D_{90} values. Specifically, the average bubble diameter decreased significantly, from 63.75 to 47.37 μm, as the SDS concentration was increased from 1 to 3 g/L. As seen in **Figure 6b**, the proportion of fine bubbles increased remarkably as the surfactant concentration increased and the bubble size distribution was shifted to smaller values and became narrower.

Similar trends have been observed in some previous studies [41, 47, 48] and this phenomenon can be attributed to the behavior of the surfactant at the liquid-gas interface. Chaphalkar et al. [47] reported that increasing the surfactant concentration reduces the interfacial tension between the gas and bulk liquid, which results in a higher probability of breakup and a decrease in bubble size.

3.3.2 Effect of XG polymer concentration

Figure 7 shows the effect of varying the XG polymer concentrations with a fixed SDS concentration of 3 g/L on the size of the CO_2 microbubbles. As can be seen in **Figure 7a**, D_{10} remained relatively constant while D_{50} and D_{90} decreased slightly as the polymer concentration was increased. Consequently, the average diameter was reduced from 55 to 47.37 μm as the XG polymer concentration went from 1 to 5 g/L. **Figure 7b** demonstrates that the bubble size distribution shifted slightly toward the lower diameter direction as the XG polymer concentration was raised. It is also apparent that the

distribution became narrower with increases in the XG polymer concentration, in agreement with literature reports [14, 29, 42]. This effect is attributed to increases in the viscosity of the solution along with the polymer concentration such that the migration of CO_2 was inhibited and smaller bubbles were obtained.

3.3.3 Effect of NaCl concentration

The effect of NaCl concentration on the size of the CO_2 microbubbles at an XG polymer concentration of 5 g/L and an SDS concentration of 3 g/L is shown in **Figure 8a**. These data confirm that increasing the NaCl concentration did not significantly affect the bubble size up to the addition of 10 g/L NaCl, with a decrease in the average diameter of only 47.38 to 46.11 μm. However, with a further increase in the NaCl concentration from 10 to 20 g/L, D_{10}, D_{50} and D_{90} all increased, while the average diameter increased to 51.90 μm. The variations in bubble size are also demonstrated in **Figure 8b**. The bubble size distribution became much broader at the highest NaCl concentration of 20 g/L and shifted to higher diameters. Interestingly, the bubble size distributions were similar at both 0 and 10 g/L NaCl. It is evident from **Figure S4g** that there was bubble coalescence at 20 g/L NaCl. The observed decrease in the average diameter of the CO_2 microbubbles at low NaCl concentrations can be attributed to the double-layer compression resulting from the presence of an electrolyte in the base solution [28, 41]. However, because higher NaCl concentrations decreased the viscosity of the solution [49], the average diameter was increased.

3.4 Changes in CO_2 microbubble size over time

One of the mechanisms responsible for increases in the bubble size over time is disproportionation or Ostwald ripening as a result of a pressure difference between two

nearby bubbles. The Laplace equation suggests that the pressure difference, P, between bubbles can be expressed as [41]:

$$\Delta P = P_1 - P_2 = 2\gamma\left(\frac{1}{r_1} - \frac{1}{r_2}\right), \quad (6)$$

where ΔP is the pressure difference between two bubbles, P_1 and P_2 are the internal pressures of bubbles with radii r_1 and r_2, respectively, and γ is the interfacial tension. A smaller bubble will have a higher internal pressure than a larger one, and so gas will diffuse from the smaller to the larger via the bulk solution. As a result, the average bubble diameter will increase as a consequence of the growth of larger bubbles and the loss of bubbles with smaller diameters [33, 41].

Figure 9 presents microscopy images of the CO_2 microbubbles in samples S1, S2 and S3 as acquired 60 min after homogenizing. The bubble size distributions are also depicted using the fitted Weibull functions. **Figure 9d** demonstrates that sample S3 had a narrower size distribution (with 3 g/L SDS) than samples S1 (1 g/L) and S2 (2 g/L). This observation indicates that the sample prepared with a higher surfactant concentration was more stable.

Figure 10 presents microscopy images of the CO_2 microbubble samples along with the bubble size distributions for specimens having different XG polymer concentrations obtained 60 min after preparation. From **Figure 10d**, it is evident that there was a greater proportion of large bubbles in sample S5 (with 1 g/L XG polymer) compared with samples S4 and S3 (3 and 5 g/L XG polymer, respectively). In addition, the diameters of the bubbles in sample S5 varied between 50 and 450 μm, while samples S3 and S4 had narrower distribution with bubble sizes in the ranges of 10 to 200 μm and 10 to 350 μm, respectively.

Figure 11 presents optical microscopy images of the CO_2 microbubbles in specimens incorporating three different NaCl concentrations, together with the BSDs obtained 60 min after preparation. As shown in **Figure 11d**, sample S7 (with 20 g/L NaCl) was less stable, as demonstrated by the more rapid increase in the proportion of large bubbles compared with the two other samples (prepared with 0 and 10 g/L NaCl). This figure also indicates that the BSD of sample S6 spanned the range of 10 to 200 μm, while the BSD of sample S7 was from 10 to 350 μm. This increase in bubble diameter resulted from aggregation and coalescence of the microbubbles with higher salt concentrations.

4 CONCLUSIONS

The present work demonstrated a new system for generating CO_2 microbubbles in conjunction with various polymer, surfactant, and salt concentrations. The results of this study indicate the following.

(1) The majority of the CO_2 microbubbles had sizes in the range of 10–100 μm and the size data were well fit using a Weibull distribution.
(2) Surfactant concentration had a considerable effect on bubble size, such that CO_2 microbubbles with smaller diameters were obtained at higher surfactant concentrations. Increasing the XG polymer concentration decreased the bubble diameters but narrowed the bubble size distributions.
(3) The mean bubble size was decreased up to a NaCl concentration of 10 g/L, while further increase in the NaCl concentration caused an increase in bubble size because of aggregation.
(4) A stability analysis of the CO_2 microbubble samples revealed that increasing the XG polymer and SDS concentrations slowed liquid drainage from the

microbubbles. The XG polymer concentration had the strongest effect on stability. Although the results indicated that the CO_2 microbubbles were most stable at an optimal salinity, the highest NaCl salt concentration gave the least stable sample because of the gravitational effect and coalescence.

(5) This work addressed substantial aspects of CO_2 microbubbles application in the EOR process, particularly the importance of stability and BSD of the pertinent materials. In addition, this study also illustrated the significance of evaluating the goodness-of-fit values for BSD models before assessing the related parameter. Such considerations have not been addressed in the previous studies[15, 19, 33, 50]. Therefore, the results obtained in this study would be beneficial to assist the development of microbubbles design in oil and gas technology.

Acknowledgements

We thank Edanz (https://jp.edanz.com/ac) for editing a draft of this manuscript.

REFERENCES

[1] Vo Thanh, H.; Sugai, Y.; Nguele, R.; Sasaki, K. Robust Optimization of CO2 Sequestration through a Water Alternating Gas Process under Geological Uncertainties in Cuu Long Basin, Vietnam. *J. Nat. Gas Sci. Eng.*, **2020**, *76* (February), 103208. https://doi.org/10.1016/j.jngse.2020.103208.

[2] Mohagheghian, E.; Hassanzadeh, H.; Chen, Z. CO2 Sequestration Coupled with Enhanced Gas Recovery in Shale Gas Reservoirs. *J. CO2 Util.*, **2019**, *34* (July), 646–655. https://doi.org/10.1016/j.jcou.2019.08.016.

[3] Azzolina, N. A.; Nakles, D. V.; Gorecki, C. D.; Peck, W. D.; Ayash, S. C.; Melzer, L. S.; Chatterjee, S. CO2 Storage Associated with CO2 Enhanced Oil

Recovery: A Statistical Analysis of Historical Operations. *Int. J. Greenh. Gas Control*, **2015**, *37*, 384–397. https://doi.org/10.1016/j.ijggc.2015.03.037.

[4] Vo Thanh, H.; Sugai, Y.; Sasaki, K. Application of Artificial Neural Network for Predicting the Performance of CO2 Enhanced Oil Recovery and Storage in Residual Oil Zones. *Sci. Rep.*, **2020**, *10* (1), 1–16. https://doi.org/10.1038/s41598-020-73931-2.

[5] Vo Thanh, H.; Sugai, Y.; Nguele, R.; Sasaki, K. Integrated Workflow in 3D Geological Model Construction for Evaluation of CO2 Storage Capacity of a Fractured Basement Reservoir in Cuu Long Basin, Vietnam. *Int. J. Greenh. Gas Control*, **2019**, *90* (August), 102826. https://doi.org/10.1016/j.ijggc.2019.102826.

[6] Lake, L. W. *Enhanced Oil Recovery*; Prentice Hall, 1989.

[7] Razavi, S. M. H.; Shahmardan, M. M.; Nazari, M.; Norouzi, M. Experimental Study of the Effects of Surfactant Material and Hydrocarbon Agent on Foam Stability with the Approach of Enhanced Oil Recovery. *Colloids Surfaces A Physicochem. Eng. Asp.*, **2020**, *585* (October 2019), 124047. https://doi.org/10.1016/j.colsurfa.2019.124047.

[8] Hashim, M. A.; Mukhopadhyay, S.; Gupta, B. Sen; Sahu, J. N. Application of Colloidal Gas Aphrons for Pollution Remediation. *J. Chem. Technol. Biotechnol.*, **2012**, *87* (3), 305–324. https://doi.org/10.1002/jctb.3691.

[9] Molaei, A.; Waters, K. E. Aphron Applications - A Review of Recent and Current Research. *Adv. Colloid Interface Sci.*, **2015**, *216*, 36–54. https://doi.org/10.1016/j.cis.2014.12.001.

[10] Zhu, W.; Zheng, X.; Li, G. Micro-Bubbles Size, Rheological and Filtration Characteristics of Colloidal Gas Aphron (CGA) Drilling Fluids for High Temperature Well: Role of Attapulgite. *J. Pet. Sci. Eng.*, **2020**, *186* (August

2019). https://doi.org/10.1016/j.petrol.2019.106683.

[11] Tabzar, A.; Arabloo, M.; Ghazanfari, M. H. Rheology, Stability and Filtration Characteristics of Colloidal Gas Aphron Fluids: Role of Surfactant and Polymer Type. *J. Nat. Gas Sci. Eng.*, **2015**, *26*, 895–906. https://doi.org/10.1016/j.jngse.2015.07.014.

[12] Alizadeh, A.; Khamehchi, E. Experimental Investigation of the Oil Based Aphron Drilling Fluid for Determining the Most Stable Fluid Formulation. *J. Pet. Sci. Eng.*, **2019**, *174* (June 2018), 525–532. https://doi.org/10.1016/j.petrol.2018.11.065.

[13] Pasdar, M.; Kamari, E.; Kazemzadeh, E.; Ghazanfari, M. H.; Soleymani, M. Investigating Fluid Invasion Control by Colloidal Gas Aphron (CGA) Based Fluids in Micromodel Systems. *J. Nat. Gas Sci. Eng.*, **2019**, *66* (March), 1–10. https://doi.org/10.1016/j.jngse.2019.03.020.

[14] Arabloo, M.; Shahri, M. P.; Zamani, M. Characterization of Colloidal Gas Aphron-Fluids Produced from a New Plant-Based Surfactant. *J. Dispers. Sci. Technol.*, **2013**, *34* (5), 669–678. https://doi.org/10.1080/01932691.2012.683989.

[15] Natawijaya, M. A.; Sugai, Y.; Anggara, F. CO2 Microbubble Colloidal Gas Aphrons for EOR Application: The Generation Using Porous Filter, Diameter Size Analysis and Gas Blocking Impact on Sweep Efficiency. *J. Pet. Explor. Prod. Technol.*, **2020**, *10* (1), 103–113. https://doi.org/10.1007/s13202-019-0680-3.

[16] Shi, S.; Wang, Y.; Li, Z.; Ding, M.; Chen, W. Experimental Study on Stability and Improving Sweep Efficiency with Microfoam in Heterogeneous Porous Media. *J. Dispers. Sci. Technol.*, **2016**, *37* (8), 1152–1159. https://doi.org/10.1080/01932691.2015.1083869.

[17] Shi, S.; Wang, Y.; Li, Z.; Chen, Q.; Zhao, Z. Laboratory Investigation of the Factors Impact on Bubble Size, Pore Blocking and Enhanced Oil Recovery with Aqueous Colloidal Gas Aphron. *J. Pet. Explor. Prod. Technol.*, **2016**, *6* (3), 409–417. https://doi.org/10.1007/s13202-015-0193-7.

[18] Sebba, F. *Foams and Biliquid Foams-Aphrons*; Wiley, Chichester, 1987.

[19] Telmadarreie, A.; Doda, A.; Trivedi, J. J.; Kuru, E.; Choi, P. CO2microbubbles - A Potential Fluid for Enhanced Oil Recovery: Bulk and Porous Media Studies. *J. Pet. Sci. Eng.*, **2016**, *138*, 160–173. https://doi.org/10.1016/j.petrol.2015.10.035.

[20] Ivan, C. D.; Quintana, J. L.; Blake, L. D. Aphron-Base Drilling Fluid: Evolving Technologies for Lost Circulation Control. *Proc. - SPE Annu. Tech. Conf. Exhib.*, **2001**, 553–558. https://doi.org/10.2523/71377-ms.

[21] Fred Growcock. Enhanced Wellbore Stabilization and Reservoir Productivity with Aphron Drilling Fluid Technology. **2004**. https://doi.org/10.2172/896513.

[22] Bjorndalen, N.; Kuru, E. Stability of Microbubble-Based Drilling Fluids under Downhole Conditions. *J. Can. Pet. Technol.*, **2008**, *47* (6), 40–47. https://doi.org/10.2118/08-06-40.

[23] Pasdar, M.; Kazemzadeh, E.; Kamari, E.; Ghazanfari, M. H.; Soleymani, M. Insight into the Behavior of Colloidal Gas Aphron (CGA) Fluids at Elevated Pressures: An Experimental Study. *Colloids Surfaces A Physicochem. Eng. Asp.*, **2018**, *537* (October 2017), 250–258. https://doi.org/10.1016/j.colsurfa.2017.10.001.

[24] Yang, E.; Fang, Y.; Liu, Y.; Li, Z.; Wu, J. Research and Application of Microfoam Selective Water Plugging Agent in Shallow Low-Temperature Reservoirs. *J. Pet. Sci. Eng.*, **2020**, *193* (October 2019), 107354. https://doi.org/10.1016/j.petrol.2020.107354.

[25] Wright, R. Jamin Effect in Oil Production. *Bull. Am. Assoc. Pet. Geol.*, **1933**, *17*, 1521–1525.

[26] Shenglong Shi, Yefei Wang, Shixun Bai, Mingchen Ding, W. C. Migration-Plugging Properties and Plugging Mechanism of Microfoam. *J. Dispers. Sci. Technol.*, **2017**, *38* (11), 1656–1664. https://doi.org/10.1080/01932691.2016.1272057.

[27] Longe, T. A. Colloidal Gas Aphrons: Generation, Flow Characterization and Application in Soil and Groundwater Decontamination, Virginia Polytechnic Institute and State University, 1989.

[28] Jauregi, P.; Gilmour, S.; Varley, J. Characterisation of Colloidal Gas Aphrons for Subsequent Use for Protein Recovery. *Chem. Eng. J.*, **1997**, *65* (1), 1–11. https://doi.org/10.1016/S1385-8947(96)03154-3.

[29] Pasdar, M.; Kazemzadeh, E.; Kamari, E.; Ghazanfari, M. H.; Soleymani, M. Insight into Selection of Appropriate Formulation for Colloidal Gas Aphron (CGA)-Based Drilling Fluids. *Pet. Sci.*, **2020**, *17* (3), 759–767. https://doi.org/10.1007/s12182-020-00435-z.

[30] Tabzar, A.; Arabloo, M.; Ghazanfari, M. H. Rheology, Stability and Filtration Characteristics of Colloidal Gas Aphron Fluids: Role of Surfactant and Polymer Type. *J. Nat. Gas Sci. Eng.*, **2015**, *26*, 895–906. https://doi.org/10.1016/j.jngse.2015.07.014.

[31] Yan, Y. L.; Qu, C. T.; Zhang, N. S.; Yang, Z. G.; Liu, L. A Study on the Kinetics of Liquid Drainage from Colloidal Gas Aphrons (CGAs). *Colloids Surfaces A Physicochem. Eng. Asp.*, **2005**, *259* (1–3), 167–172. https://doi.org/10.1016/j.colsurfa.2005.02.028.

[32] Nguyen Hai Le, N. N. H.; Sugai, Y.; Sasaki, K. Investigation of Stability of CO2

Microbubbles—Colloidal Gas Aphrons for Enhanced Oil Recovery Using Definitive Screening Design. *Colloids and Interfaces*, **2020**, *4* (2), 26. https://doi.org/10.3390/colloids4020026.

[33] Pasdar, M.; Kazemzadeh, E.; Kamari, E.; Ghazanfari, M. H.; Soleymani, M. Monitoring the Role of Polymer and Surfactant Concentrations on Bubble Size Distribution in Colloidal Gas Aphron Based Fluids. *Colloids Surfaces A Physicochem. Eng. Asp.*, **2018**, *556* (August), 93–98. https://doi.org/10.1016/j.colsurfa.2018.08.020.

[34] Sadeghialiabadi, H.; Amiri, M. C. Toward the Effects of the Geometric and Operating Parameters on Colloidal Gas Aphron Stability. *J. Dispers. Sci. Technol.*, **2015**, *36* (11), 1621–1627. https://doi.org/10.1080/01932691.2014.987782.

[35] Tabzar, A.; Ziaee, H.; Arabloo, M.; Ghazanfari, M. H. Physicochemical Properties of Nano-Enhanced Colloidal Gas Aphron (NCGA)-Based Fluids. *Eur. Phys. J. Plus*, **2020**, *135* (3). https://doi.org/10.1140/epjp/s13360-020-00174-5.

[36] Chen, X.; Hussein, M.; Becker, T. Determination of Bubble Size Distribution in Gas–Liquid Two-Phase Systems via an Ultrasound-Based Method. *Eng. Life Sci.*, **2017**, *17* (6), 653–663. https://doi.org/10.1002/elsc.201500148.

[37] Moradi, M.; Alvarado, V.; Huzurbazar, S. Effect of Salinity on Water-in-Crude Oil Emulsion: Evaluation through Drop-Size Distribution Proxy. *Energy and Fuels*, **2011**, *25* (1), 260–268. https://doi.org/10.1021/ef101236h.

[38] Maaref, S.; Ayatollahi, S. The Effect of Brine Salinity on Water-in-Oil Emulsion Stability through Droplet Size Distribution Analysis: A Case Study. *J. Dispers. Sci. Technol.*, **2018**, *39* (5), 721–733. https://doi.org/10.1080/01932691.2017.1386569.

[39] Rajeev Parmar, S. K. M. Terminal Rise Velocity, Size Distribution and Stability of Microbubble Suspension. *Asia-Pacific J. Chem. Eng.*, **2015**, *10* (3), 450–465. https://doi.org/https://doi.org/10.1002/apj.1891.

[40] Alam, R.; Shang, J. Q.; Khan, A. H. Bubble Size Distribution in a Laboratory-Scale Electroflotation Study. *Environ. Monit. Assess.*, **2017**, *189* (4). https://doi.org/10.1007/s10661-017-5888-4.

[41] Xu, Q.; Nakajima, M.; Ichikawa, S.; Nakamura, N.; Roy, P.; Okadome, H.; Shiina, T. Effects of Surfactant and Electrolyte Concentrations on Bubble Formation and Stabilization. *J. Colloid Interface Sci.*, **2009**, *332* (1), 208–214. https://doi.org/10.1016/j.jcis.2008.12.044.

[42] Arabloo, M.; Pordel Shahri, M. Experimental Studies on Stability and Viscoplastic Modeling of Colloidal Gas Aphron (CGA) Based Drilling Fluids. *J. Pet. Sci. Eng.*, **2014**, *113*, 8–22. https://doi.org/10.1016/j.petrol.2013.12.002.

[43] Pinho, H. J. O.; Mateus, D. M. R.; Alves, S. S. Probability Density Functions for Bubble Size Distribution in Air–Water Systems in Stirred Tanks. *Chem. Eng. Commun.*, **2018**, *205* (8), 1105–1118. https://doi.org/10.1080/00986445.2018.1434159.

[44] Stephens, M. A. EDF Statistics for Goodness of Fit and Some Comparisons. *J. Am. Stat. Assoc.*, **1974**, *69* (347), 730–737. https://doi.org/10.1080/01621459.1974.10480196.

[45] Pasdar, M.; Kazemzadeh, E.; Kamari, E.; Ghazanfari, M. H.; Soleymani, M. Insight into the Behavior of Colloidal Gas Aphron (CGA) Fluids at Elevated Pressures: An Experimental Study. *Colloids Surfaces A Physicochem. Eng. Asp.*, **2018**, *537* (May 2018), 250–258. https://doi.org/10.1016/j.colsurfa.2017.10.001.

[46] Hosseini-Kaldozakh, S.; Khamehchi, E.; Dabir, B.; Alizadeh, A.; Mansoori, Z.

Experimental Investigation of Water Based Colloidal Gas Aphron Fluid Stability. *Colloids and Interfaces*, **2019**, *3* (1), 31. https://doi.org/10.3390/colloids3010031.

[47] Chaphalkar, P. G.; Valsaraj, K. T.; Roy, D. A Study of the Size Distribution and Stability of Colloidal Gas Aphrons Using a Particle Size Analyzer. *Sep. Sci. Technol.*, **1993**, *28* (6), 1287–1302. https://doi.org/10.1080/01496399308018037.

[48] Ahmadi, M. A.; Galedarzadeh, M.; Shadizadeh, S. R. Colloidal Gas Aphron Drilling Fluid Properties Generated by Natural Surfactants: Experimental Investigation. *J. Nat. Gas Sci. Eng.*, **2015**, *27*, 1109–1117. https://doi.org/10.1016/j.jngse.2015.09.056.

[49] Keshavarzi, B.; Mahmoudvand, M.; Javadi, A.; Bahramian, A.; Miller, R.; Eckert, K. Salt Effects on Formation and Stability of Colloidal Gas Aphrons Produced by Anionic and Zwitterionic Surfactants in Xanthan Gum Solution. *Colloids and Interfaces*, **2020**, *4* (1), 9. https://doi.org/10.3390/colloids4010009.

[50] Zhu, W.; Zheng, X.; Li, G. Micro-Bubbles Size, Rheological and Filtration Characteristics of Colloidal Gas Aphron (CGA) Drilling Fluids for High Temperature Well: Role of Attapulgite. *J. Pet. Sci. Eng.*, **2020**, *186* (August 2019), 106683. https://doi.org/10.1016/j.petrol.2019.106683.

Figure 1 Schematic diagram of the preparation of CO_2 microbubbles: (1) Homogenizer, (2) Polymer and surfactant solution, (3) Porous stone (gas diffuser), (4) Gas flow meter, (5) Pressure regulator, (6) CO_2 gas tank

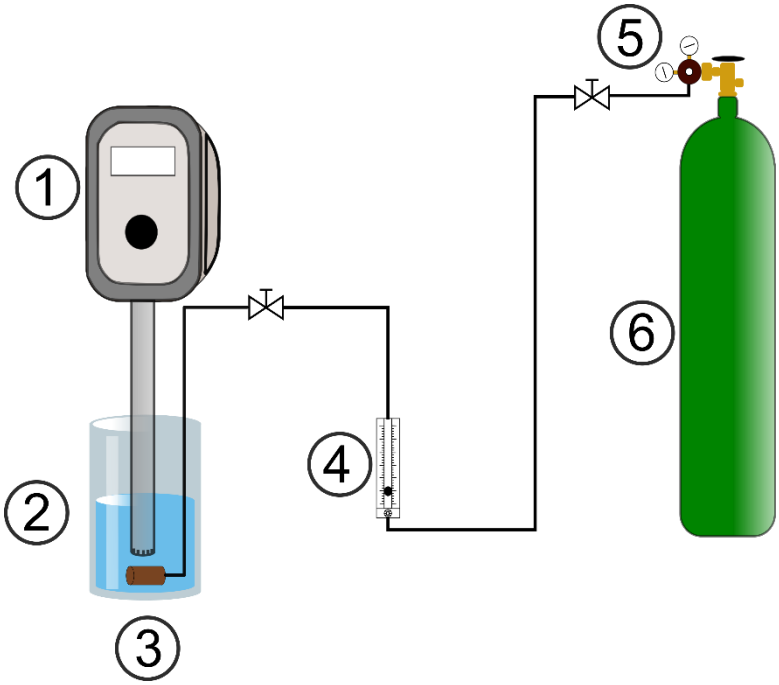

Figure 2 Microscopic image and schematic view of a CO_2 microbubble

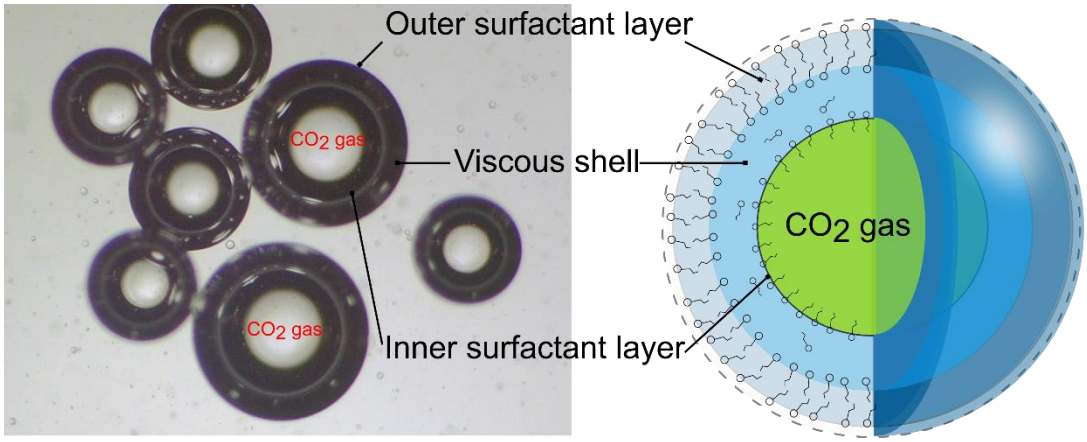

Figure 3 Effect of SDS concentration on the stability of CO_2 microbubbles (with 0 g/L XG)

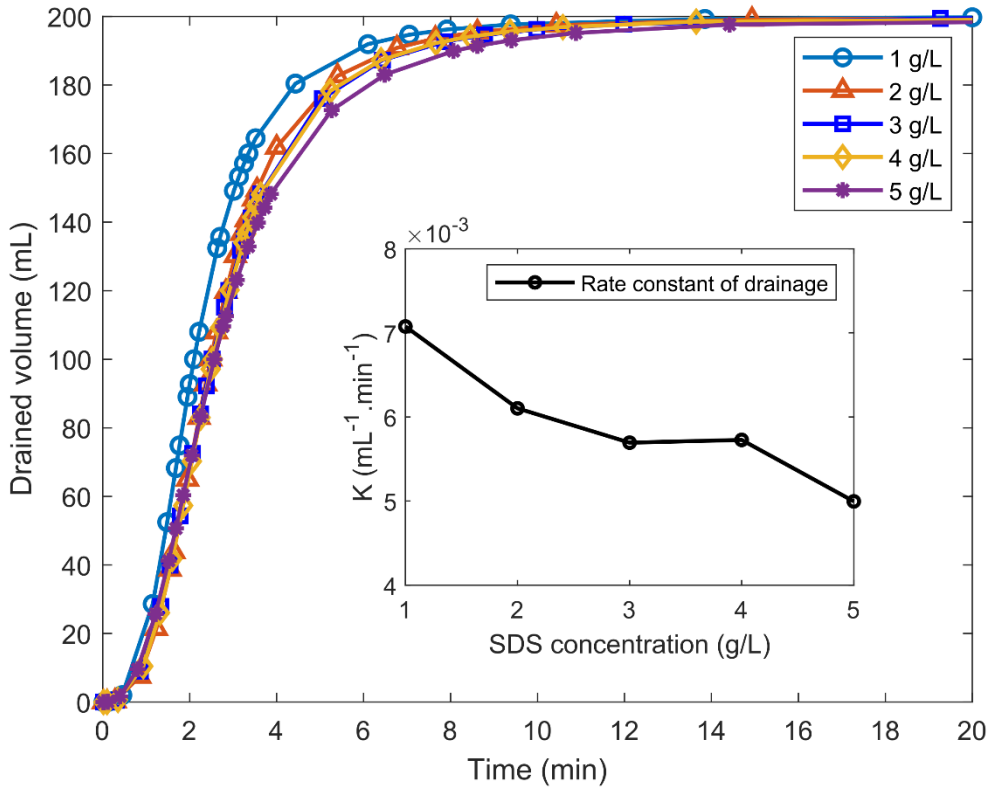

Figure 4 Effect of XG concentration on the stability of CO_2 microbubbles (with 3 g/L SDS)

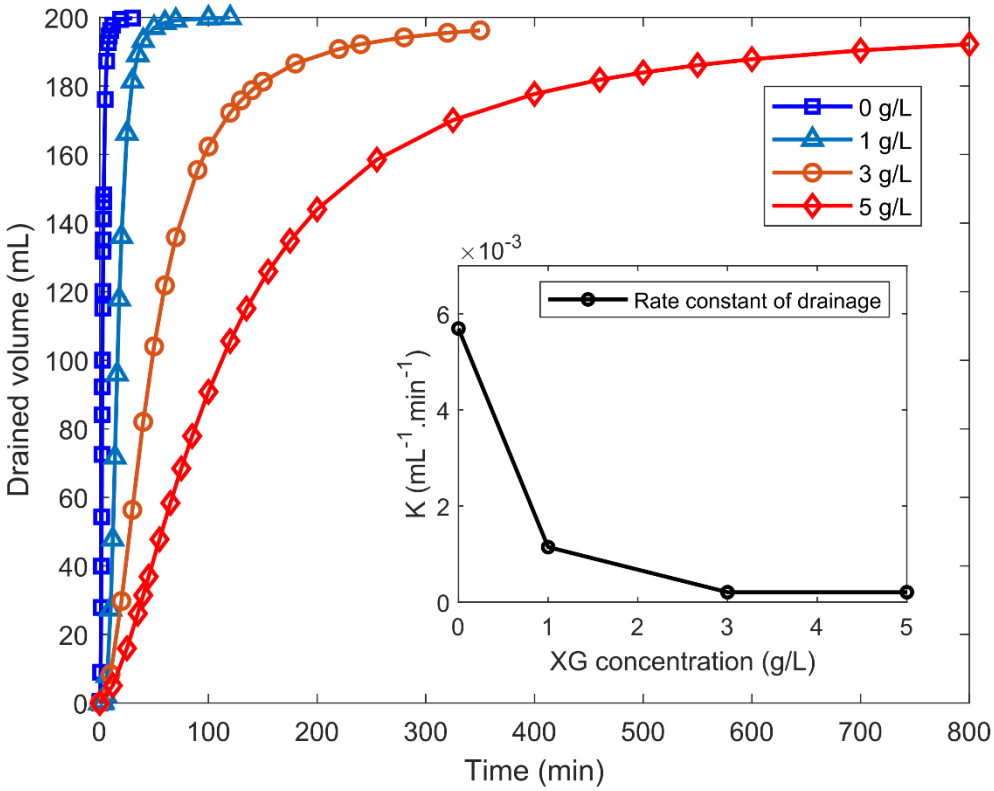

Figure 5 Effect of NaCl concentration on the stability of CO_2 microbubbles (with 3 g/L SDS and 5 g/L XG)

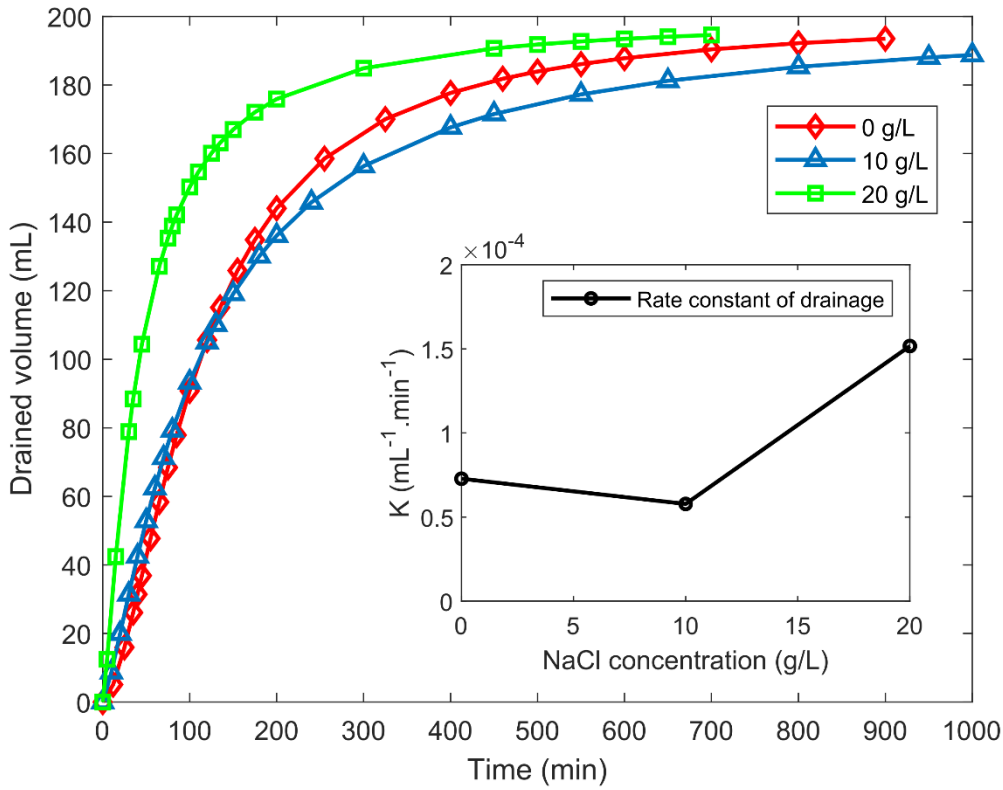

Figure 6 Influence of SDS concentration (1, 2, 3 g/L) upon bubble size. (b) BSD at three SDS concentrations, experimental and fitted results are represented using icons and solid lines, respectively

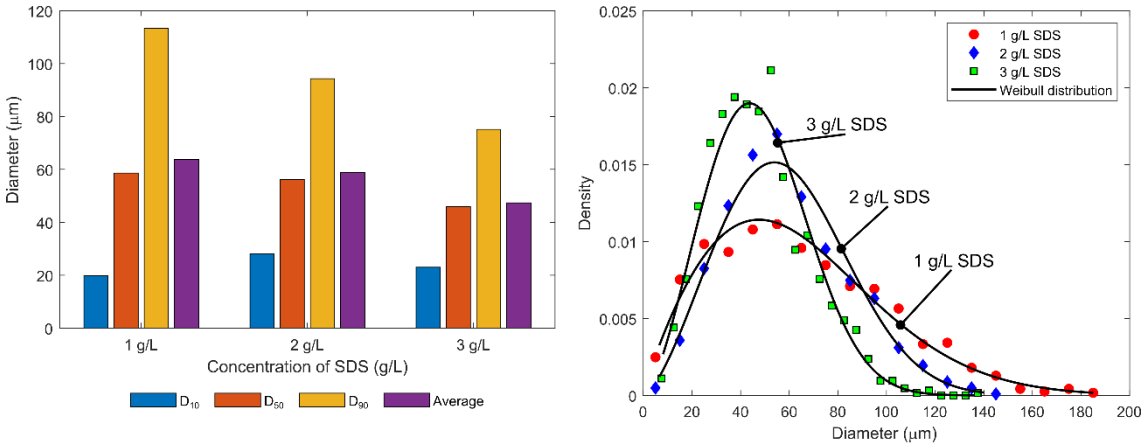

(a) (b)

Figure 7 Influence of XG concentration (1,3,5 g/L) upon bubble size. (b) BSD at three XG concentrations, experimental and fitted results are represented using icons and solid lines, respectively

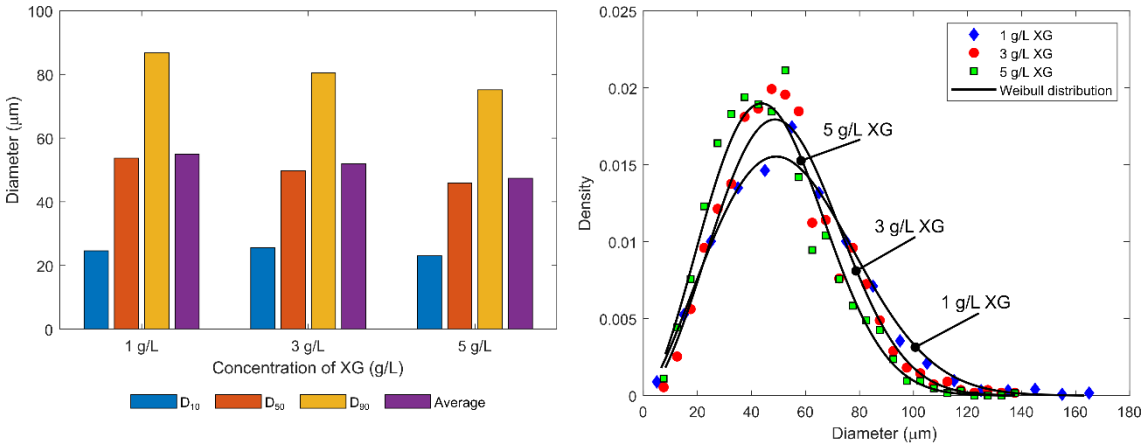

Figure 8 (a) Influence of NaCl concentration (0, 10, 20 g/L) upon bubble size. (b) BSD at three NaCl concentrations, experimental and fitted results are represented using icons and solid lines, respectively

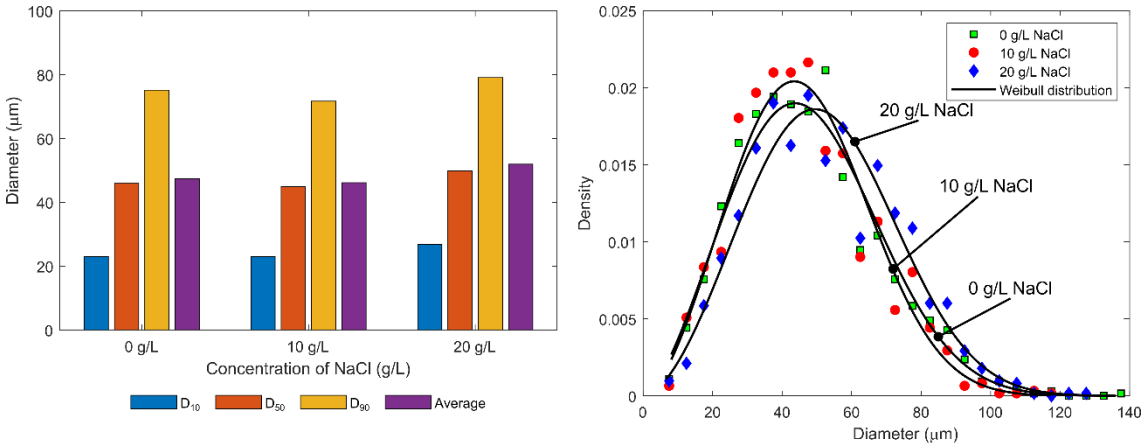

(a) (b)

Figure 9 Microscopic views of CO_2 microbubbles samples, 60 minutes after preparation (a) S1 sample, (b) S2 sample, (c) S3 sample. And (d) Bubble size distribution functions.

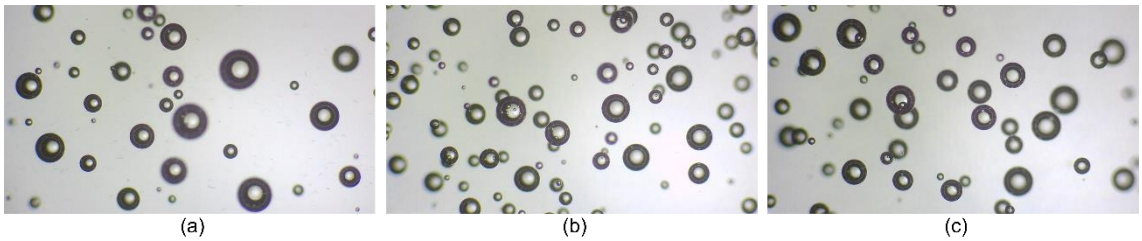

(a) (b) (c)

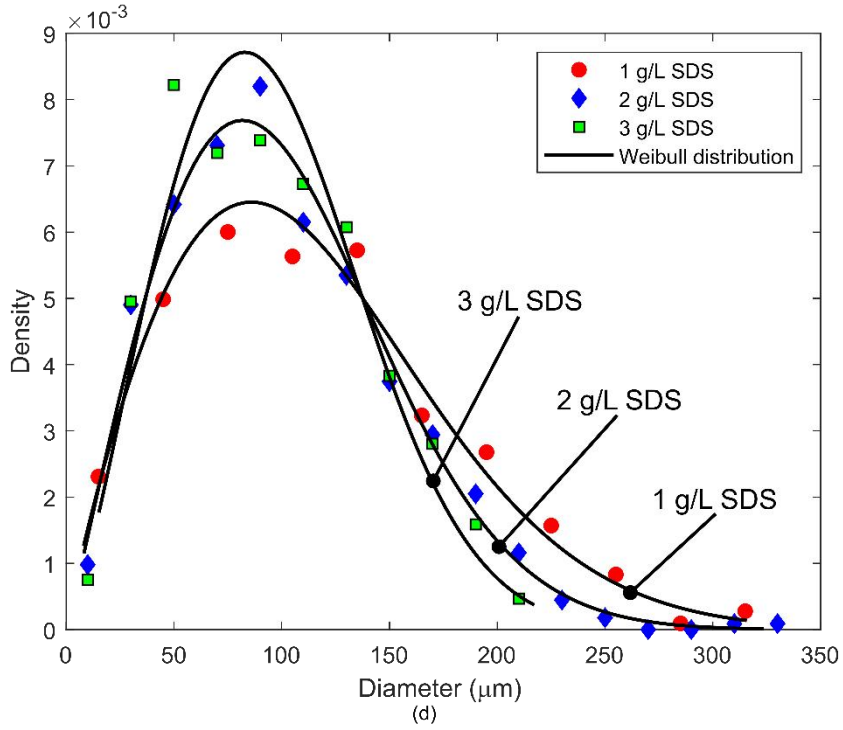

(d)

Figure 10 Microscopic views of CO_2 microbubbles samples, 60 minutes after preparation (a) S5 sample, (b) S4 sample, (c) S3 sample. And (d) Bubble size distribution functions.

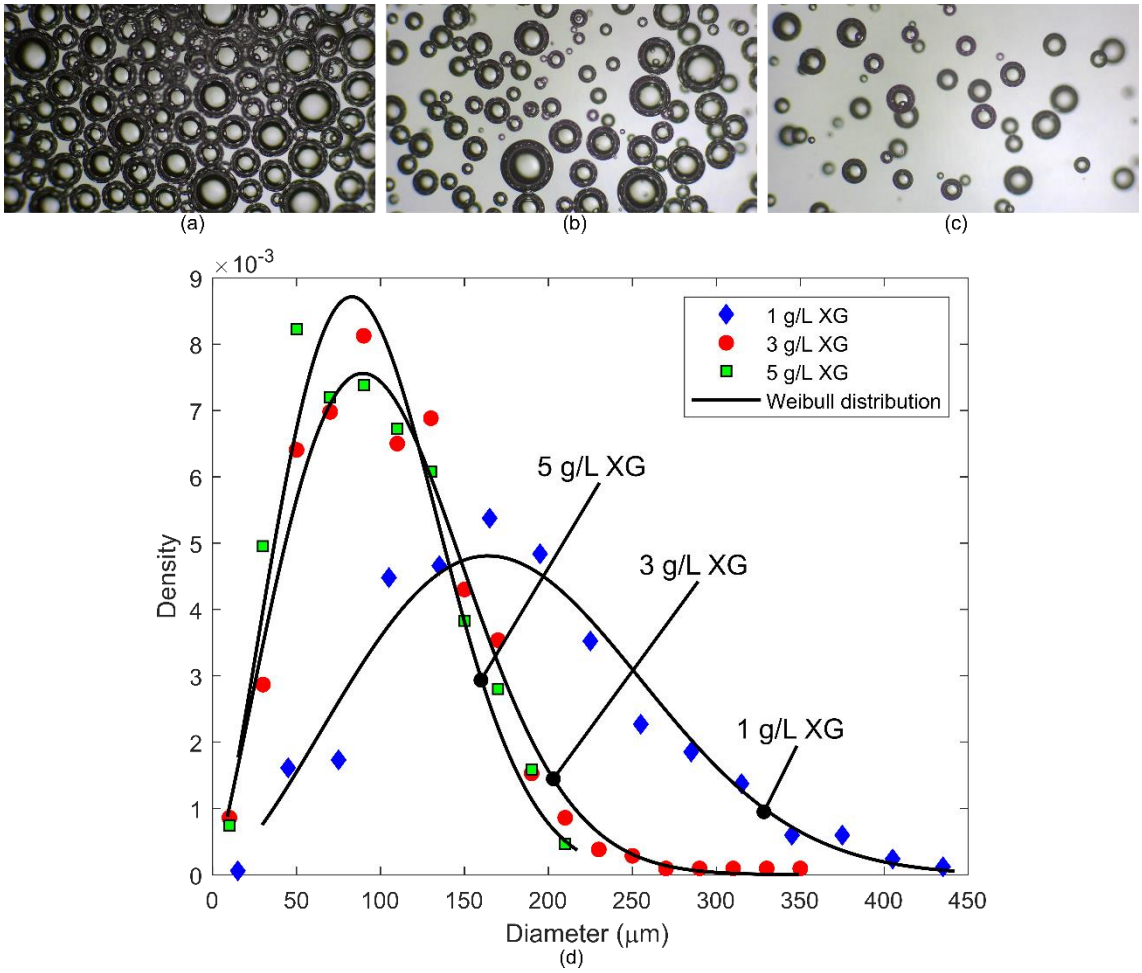

Figure 11 Microscopic views of CO_2 microbubbles samples, 60 minutes after preparation (a) S3 sample, (b) S6 sample, (c) S7 sample. And (d) Bubble size distribution functions.